Article

DNA Tetrahedron Based Biosensor for Argonaute2 Assay in Single Cells and HIV-1 Related Ribonuclease H Detection in Vitro

Kai Zhang, Wanting Huang, Yue Huang, Hao Li, Ke Wang, Xue Zhu, and Minhao Xie

Anal. Chem., **Just Accepted Manuscript** • DOI: 10.1021/acs.analchem.9b00011 • Publication Date (Web): 03 May 2019

DNA Tetrahedron Based Biosensor for Argonaute2 Assay in Single Cells and HIV-1 Related Ribonuclease H Detection in Vitro

Kai Zhang,[*,a] *Wanting Huang,*[a] *Yue Huang,*[b] *Hao Li,*[c] *Ke Wang,*[a] *Xue Zhu,*[a] *Minhao Xie,* [*, a]

[a]*Key Laboratory of Nuclear Medicine, Ministry of Health, Jiangsu Key Laboratory of Molecular Nuclear Medicine, Jiangsu Institute of Nuclear Medicine. Wuxi, Jiangsu 214063, China.*

[b]*College of Light Industry and Food Engineering, Nanjing Forestry University, Nanjing, Jiangsu 210037, China*

[c]*School of Biological Science and Technology, University of Jinan, No. 106 Jiwei Road, Jinan, Shandong 250022, China*

* Corresponding author. Fax: +86-510-85508775; Tel: +86-510-85508775

E-mail addresses: zhangkai@jsinm.org (K. Zhang), xieminhao@jsinm.org (M. Xie)

Abstract: A well-designed DNA tetrahedron based biosensor (DTB) has been employed for imaging and detection of Argonaute2 (Ago2), a key RNA interference (RNAi) protein. This DTB mainly contains two segments: DNA tetrahedron as a frame and a photo-induced electron transfer (PET) pair as a fluorescence transducer. The DNA tetrahedral nanostructure is assembled with four nucleic acid strands. On one edge, one DNA strand forms a hairpin structure (RNA sequence) which is implanted in the two complementary double strand DNA. And, the PET pairs, DNA/AgNC and G-quadruplex/hemin complex are labeled at the two terminuses of another DNA strand, respectively. The DNA tetrahedron structure forms a switchable scaffold that can present the functional DNA motifs in two different modes, according to the presence/absence of the target protein. The cleavage reaction by Ago2/miR-21 complex opens the hairpin structure, leading the PET pairs separated to each other in the spatial sate. Thus, the DNA/AgNC fluorescence can be measured. By using this DTB, we obtained the 4.54 nM Ago2 detection limit and successful assay Ago2/miR-21 complex in living cells. Also, the DTB was successful employed for the further assay RNase H, which plays an importance role in HIV-1 reverse transcriptase pathway, with a limit of detection (LOD) 3.41 U mL^{-1}. Our DTB can be used as a device for the imaging protein concentration in single cells, and have a potential value for disease diagnosis and treatment.

INTRODUCTION

Proteins, nucleic acids or small molecules research in living cells can offer deep comprehension of cellular biological pathway in single cells.[1] Therefore, assay these

valuable biomolecules expression levels in living cell has great benefit in early disease treatment and cancer diagnosis.[2-6] Up to date, many strategies have been reported to assay their levels, including qPCR technology, and Western blotting.[7,8] Nevertheless, these approaches are labor-intensive and time-consuming. In order to solve these issues, various strategies for bio-molecule assay and imaging in living cells have been developed.[9, 10] In comparison with the qPCR and Western blotting technologies, bio-molecules assay and imaging in living cell has the advantages of direct visualization, easy operating and high sensitivity.

On the other hand, RNA interference (RNAi) is a recently discovered molecular mechanism that has greatly expanded our traditional view of gene expression and regulation. [8,11,12] In this mechanism, short single stranded RNA, known as small interfering RNA (siRNA), chaperoned by specific proteins such as Argonaute2 (Ago2), can specifically target certain message RNA (mRNA) strands and digest them into fragments without mRNA function, namely, the transportation of nuclear gene encoding information into the cytoplasm. [13-15] This "RNAi" mechanism has been found ubiquitously present in all cell and tissue types inhibiting protein expression.[16-18] Although it can currently be said that a large part of RNAi has been delineated, our understanding of it is still far from comprehensive and thorough, this less satisfactory condition may, to some extent, be due to practical and technical problems encountered in applying traditional nucleic acid probes in RNAi study.

RNA is a rather transient species in common cellular life, it's constantly synthesized and digested with a very short half-life.[13, 15] So nucleic acid probes for RNA study must achieve higher cellular up-take rate and be more robust when subject to potential cellular enzymatic digestion. In these aspects, traditional probes of simple strand configuration is usually short of expectation.[19-20] Because of their unknown origin, these probes often meet a hostile treat from the target cells. The up-take of these strands are highly restricted, while their cellular distribution, after being engulfed by the cells,

are still very limited, since they are usually enclosed by lipid lined vesicles.[9] In this manner, a cell has, in effect, banned those alien nucleic acids from even getting into contact with the cytoplasmic enzymes and nano-machinery such as Ago2 and its accompanying siRNA sequence miR-21. The fate awaiting such "jailed" probes are usually enzymatic digestion inside the vesicles, the simple strand structures of these probes can offer little resistance and protection from such treatments. Therefore, more robust nucleic acid probes are now needed for obtaining information on cellular RNA activities of higher quality, which is a prerequisite for furthering our understanding of RNAi.

Such a robust nucleic acid probe may be constructed using recent development in manipulating bio-macro-molecules: the last decade has witnessed an unparalleled advance in using the natural building block of genome, namely DNA, to form structurally ordered nano architectures that are collectively known as "DNA origami".[21-25] Among various types of DNA origami constructions are a simplest and robust type called "DNA tetrahedron". Such a tetrahedron is usually formed by four separate strands pieced together through base-pairing. The tetrahedron so formed possesses very high structural stiffness, and because this architecture is previously never encountered by natural proteins, they usually cannot effectively digest such tetrahedrons, giving them high resistance against nuclease attack.[26-29] Moreover, recent studies have confirmed that the cellular up-take of DNA tetrahedron can proceed effectively even without the assistance of transfection agents.[30-35] Taken together, these features of DNA tetrahedron may herald promising application of it as a powerful cellular probe for RNAi study.

Here we have designed such a probe to demonstrate the above proposed strategy of using DNA tetrahedron as molecular scaffold for a biosensor: In the assembled tetrahedron, there are six edges, and our design chose one such edge to present on it the functional probe sequence, while the remaining five will preserve the structural robustness that is essential for a DNA tetrahedron's high survival rate against cellular environmental hazard. The "functional" edge is labeled blue in scheme 1, and this segment is actually formed by the base-pairing between parts of DNA3 and DNA4.

Within this segment, two single-stranded terminal pendant have been designed at the two termini of DNA4. On one terminal pendant is designed a sequence that can form into G-quadraplex (G4) when properly pre-incubated with potassium ion; while on the other is constructed a terminal motif that can induce the in-situ formation of silver nano-cluster (AgNC) on it, the size of the cluster is small enough for it to be employed as a quantum dot or fluorescent signal reporter. If this signal reporter motif were brought to the vicinity of the G4 motif, photo-induced electron transfer (PET) can take place, keeping the former quenched by the latter motif. [36,37] This feature is exploitable for designing a switchable photo-probe: a self stem-looping sequence is constructed on DNA3, as shown in Scheme 1, loop-forming of this motif (hairpin structure) can place the signal reporter and G4 motifs closely enough to each other to induce quenching. Besides this initial quenching that enables the desirable "signal-on" working mode, this loop-forming also has shortened the blue leg of the tetrahedron, therefore bracing the whole structure in a relatively "closed" conformation possessing an intrinsic trend to expand on this shortened side. In the presence of Ago2 protein and miR-21 RNA, this loop can be digested by the Ago2/miR-21 complex, and then the intrinsic structural stiffness of the tetrahedron will stretch the whole tetrahedral structure into a more open conformation, leaving the G4 and signal reporter spatially separated so the fluorescence of the signal reporter can be restored. The above-proposed mechanism of fluorescent sensing is mainly based on fluorescent resonance energy transfer, or the so-called PET, this gives a very low fluorescent background, while the restoration of fluorescence can only be triggered by the target protein catalyzed re-opening of the tetrahedron structure, ensuring a low rate of false positive results. Based on this, we employed our well-designed tetrahedron based biosensor (DTB) for the detection and imaging of Ago2 in single-cell and Ribonuclease H (RNase H) *in vitro*.

EXPERIMENTAL SECTION

Reagents. Argonaute1 (Ago1), argonaute2 (Ago2), and argonaute3 (Ago3) were obtained from Sino Biological Inc (Beijing, China). Diethyl pyrocarbonate (DEPC) and

Tris (2-carboxyethyl) phosphine hydrochloride (TCEP) were purchased from Sigma-Aldrich Inc. (St. Louis, Missouri, USA). DNase I endonuclease, HeLa cells was obtained from KeyGen Biotech. Co. Ltd. (Nanjing, China). RNasin, Gel electrophoresis and loading buffer were purchased from Takara Biotech. Co. Ltd. (Dalian, China). All solutions in this report were prepared using ultrapure water (> 18 MΩ cm, Milli-Q, Millipore). The strand sequences were purchased from Genscript Biotech. Co., Ltd. (Nanjing, China) with the sequences as shown in Table 1.

In order to maintain the environment in this work with RNase-free, the solutions were prepared with ddH_2O which were treated with 0.1% DEPC and 1 U μL^{-1} RNasin for Ago2 assay.

Preparation of DTB and Fluorescent Ago2 assay. 1 μM strands of DNA1, DNA2, DNA3, and DNA4 for the formation of the DTB (with the final concentration of 1 μM) were mixed in phosphate buffer (5.0 mM $Mg(Ac)_2$, pH 7.4) at 95 °C and then rapidly cooled to 4 °C. The solution of DTB was then added with $AgNO_3$ (1 μL, 6 mM,). Then, the $AgNO_3$ incubated DTB was stirring for 20 min in dark on the ice bath, before reduced with $NaBH_4$ (1 μL, 6 mM, $AgNO_3/NaBH_4$=1:1, molar ratio) for 2 h at room temperature in the dark. The prepared DTB was reduced at 4 °C for another 12 h. The synthesized DTB was then centrifuged by using Nanosep Centrifugal Devices (30K, molecular weight cutoffs) with 2320×g for 10 min. The obtained solution containing DTB was dissolved in PBS buffer (with 0.1% DEPC and 1 U μL^{-1} RNasin) for further application. Then 1.0 μM hemin and 50 mM KNO_3 were added to the prepared DTB solution, and the DTB/hemin mixture was incubated for another 2 h at

room temperature. After treated with different concentration Ago2 (with 1 μM miR-21, equally to the DTB concentration) at 37 °C for 30 min, the fluorescence spectrum was recorded.

Polyacrylamide Gel Electrophoresis (PAGE). The strand solutions mixed with 6× loading buffer (TEK buffer, pH 8.0, 50% glycerol, 0.25% bromphenol blue) were carried out in nondenaturing polyacrylamide gel electrophoresis (PAGE) (10%) in 1× TBE (12.5 mM Mg^{2+}, pH 8.0) buffer at a 120 V constant voltage for 1.5 h at 4 °C. The gel was taken photograph under UV light (ChemiDoc MP, Bio-Rad) after staining with GelRed for 15 min. The concentration of each strand is 1 μM. For Ago2 digestion assay, DTB was treated with 1 μM miR-21 for 30 min, then the DTB/miR-21 complex treated with 100 nM Ago2 for another 30 min.

Cell culture. HeLa cells were cultured with 10% fetal calf serum (FCS, Sigma), penicillin (100 μg mL^{-1}), and streptomycin (100 μg mL^{-1}) in a flask in DMEM (GIBCO) at 37 °C in a humidified atmosphere containing 5% CO_2.

Ago2 assay in cell lysates. HeLa cells were collected in the exponential phase of growth with the number of 1×10^6. After washed twice with ice-cold PBS (0.1 M, pH 7.4), cells were resuspended in ice-cold CHAPS lysis buffer (50 μL) which containing 10 mM Tris-HCl (pH 7.5), 1 mM EGTA, 1 mM $MgCl_2$, 0.1 mM PMSF, 0.5% CHAPS and 10% glycerol. After incubating 30 min on ice, the mixture was centrifuged at 23755×g at 4 °C for another 20 min. The supernatant was collected and diluted to 50 μL and storage at -80 °C for future use.

For the Ago2 assay in cell extract, different concentration of Ago2 (10 μL) added into the cell lysates extract. After incubating the mixtures with 100 μL DTB at 37 °C for 30 min, the fluorescent intensity was recorded.

Image Ago2 in single-cell. 0.5 mL HeLa cells (1×10^6 mL^{-1}) were seeded to confocal dish for 24 h culture, and 25 μL DTB was then added into the confocal dish. After incubation at 37 °C for 6 h, the DTB treated HeLa cells were sent for fluorescent confocal imaging assay.

Ago2 knockdown. Ago2 knockdown in HeLa cell lines was performed by transfecting a siRNA duplex (siRNA1 and siRNA2, Table 1) using Lipofectamine 3000 (Invitrogen, Grand Island, NY, USA) following the manufacturer's instructions. Briefly, after cultured in dish for 24 h, 0.5×10^6 cells transfected with siRNA duplex: 5 μL of 500 amol siRNA duplex diluted in 125 μL Opti-MEM Medium reduced serum media. And, 4 μL Lipofectamine 3000 was diluted in 125 μL Opti-MEM Medium reduced serum media. Then added diluted siRNA duplex concentration to diluted Lipofectamine 3000 concentration and incubated at room temperature for 15 minutes. After the incubation, added the mixture to the cultured cells and incubated the cells for 48 h before DTB incubation.

RT-qPCR analysis for c-Myc RNA. Total RNA samples were extracted from HeLa cells (or Ago2 knockdown HeLa cells) using a Trizol reagent (Invitrogen, Beijing, China) according the manufacturer's instructions in RNase-free H_2O. Total RNA samples (1 μg per reaction) were reversely transcribed into cDNAs by using SuperScript™ First-Strand Synthesis System (Invitrogen). Then, RT-qPCR was

performed by using the cDNA, which employed SYBR green PCR Master Mix (Takara, Shiga, Japan). Each amplification reaction underwent denaturation at 95 °C for 30 s, amplification for 40 cycles at 95 °C for 10 s, annealing and extension at 60 °C for 20 s using ABI7500 sequence detection system (Life Technologies, ON, USA). The primers of mRNA forward (5'-GCCACGTCTCCACACATCAG-3') and mRNA reverse (5'-TGGTGCATTTTCGGTTGTTG-3') were used. In all experiments, the human glyceraldehyde-3-phosphate dehydrogenase (GAPDH) was used as an internal control in RT-qPCR amplification, its forward primer (5'-GGTCTCCTCTGACTTCAACA-3') and reverse primer (5'-AGCCAAATTCGTTGTCATAC-3') were employed for the RT-qPCR amplification reaction.

RNase H assay in vitro. The solutions for the RNase H assay were prepared with BeyoPure™ Ultrapure Water (DNase/RNase-Free, Sterile). After treated with different concentration of RNase H (with 1 μM Antisense oligonucleotide (ASO)) at 37 °C for 30 min, the fluorescence spectrum of the DTB solution was recorded. For the RNase H assay in cell extract, different concentration of RNase H (10 μL) added into the cell lysates extract. After incubating the mixtures with 100 μL DTB at 37 °C for 30 min, the fluorescent intensity was recorded.

Apparatus. The cell images were obtained on TCS SP5 laser scanning confocal microscope (Leica, Germany). The fluorescence spectra were obtained on RF-5301PC spectrofluorophotometer (Shimadzu, Japan). The cytometric analysis was performed on a FC500 Cytometer (Beckman Coulter, United States).

RESULTS AND DISCUSSION

The working principle. We fabricated a PET based biosensor for ultrasensitive detection of Ago2 concentration in living-cell based on a well-designed tetrahedral DNA nanostructure. The application of tetrahedral DNA nanostructure makes itself become an effective intracellular machinery that can penetrate cells without extra transfection agents due to its appropriate size and desirable biocompatibility. The DNA tetrahedral nanostructure is assembled with four nucleic acid strands, DNA1, DNA2, DNA3, and DNA4. Each edge has two complementary double strand DNA. On one edge, DNA3 forms a hairpin structure (RNA sequence) which is embedded in the two complementary double strand DNA. And, the PET pairs, DNA/AgNC and G4 are labeled at the two terminus of the DNA4, the DNA3 complementary, respectively. Particularly, the hairpin structure of DNA3, acts as recognition part, can be cleaved by Ago2/miR-21 complex. The cleavage reaction makes the hairpin structure in a free stage, leading the two PET pair spatially separated (PET off). In this state, the DNA/AgNC fluorescence can be observed when excited with the light of 560 nm. However, in the absence of the Ago2/miR-21 complex, the formation of the hairpin structure on DNA3 leads the two PET pairs adjacent to each other. (PET on). In this state, the DNA/AgNC fluorescence quenched by G4 when excited at 560 nm irradiation. Thus, the fluorescence intensity of DNA/AgNC can be used as a signal transducer for quantitation of Ago2 concentration.

Feasibility study. The construction of the DTB was verified by native polyacrylamide gel electrophoresis (PAGE) (Figure 1A). As different strands or duplexes were added from lane 1 to lane 7, the DNA tetrahedral nanostructure in lane

g migrated more slowly than other single strand and other DNA duplexes (lanes 1-7) due to the steric hindrance and its huge molecular weight. These results demonstrated that the DNA strands interacted with each other effectivity. In addition, the DTB/miR-21 complex formation and the hairpin structure cleavage reactions were also investigated. As shown in Figure 1B, after the miR-21 addition, there was a new band observed on the top of lane 2, which indicated the formation of DTB/miR-21 complex. After incubating with Ago2, the bands in lane 3 were similar to lane 1 (hairpin structure cleaved DTB *vs* DTB), but another obvious new band appeared (miR-21), indicated the successful Ago2/miR-21 cleavage reaction.

The length of the stem part of the hairpin structure in DNA3 was important for the fluorescence recovery. The tetrahedral DNA nanostructure was formed using a series of DNA3 by changing the length of the stem part from one to eight bases. We chose the fluorescence intensity ratio (the fluorescence intensity obtained by incubating with Ago2 (300 nM)/miR-21 (1 μM) complexes (F_{signal}) and the fluorescence intensity obtained before incubating with Ago2/miR-21 complexes (F_{blank}) to calculate the fluorescence intensity changes. As shown in Figure 1C, the best fluorescence intensity change was obtained when the length was four bases. This phenomenon may be caused by the stem's stability, which leads to the high fluorescence intensity in the absence of Ago2/miR-21 complex. Even we obtained high fluorescence intensities after the addition of Ago2/miR-21 complexes, the ratio of the F_{signal}/F_{blank} were low. The five to eight bases length of the stem may cause the hairpin structure stable enough before the addition of Ago2/miR-21 complex, however, after the addition of Ago2/miR-21

complexes, the cleavage of the hairpin could not make the AgNC far away from the G4 since the high T_m value of the hybridization part. The ratio of the F_{signal}/F_{blank} were also low. Therefore, we chose four bases length to build the biosensor.

To understand the time-dependent Ago2/miR-21 complex cleavage reaction, we employed two concentrations of Ago2 (10 and 100 nM) to study the kinetic reaction. The fluorescence intensity changes rapidly in the first 10 min and reach the plateau at the 30 min (Figure 1D). Thus, we chose the 30 min for the Ago2/miR-21 complex incubation time.

Sensitivity of the DTB for the assay Ago2 concentration. The DNA tetrahedral biosensor (DTB) was first employed to assay Ago2 concentration in solution. Combined Ago2/miR-21 complexes (different concentration of Ago2 treated with 1 μM miR-21) were added to the DNA tetrahedrons biosensor solution, and the DNA/AgNC fluorescence intensity were recorded (fluorescence emission at 620 nm with the excitation at 560 nm). From the Figure 2A, we can obtain that the fluorescence intensity variation was dependent upon the addition of the Ago2/miR-21 complex concentration. A gradual increase in DNA/AgNC fluorescence intensity with increasing Ago2 concentration with the range of 0 to 500 nM. The linear relationship between the DNA/AgNC fluorescence intensity (FL) and the concentration of Ago2 (C_{ago2}) with the range from 0 to 100 nM by using an equation $FL = 4.40\ C_{ago2} + 211.77$ ($R^2 = 0.9950$) (Figure 2B insert). The detection limit of 4.54 nM could be obtained by according to the 3σ method (the responses of the blank tests plus 3 times the standard deviation). Its sensitivity is comparable to other previous report (Table S1).

Specificity assay by using the DTB for the assay Ago2 concentration. The specificity of the proposed DTB was evaluated with two control experiments: (1) control experiments that employed two Ago2 analogues (argonaute1 (Ago1) and argonaute3 (Ago3) (100 nM each)) and other endonucleases (RNase H and Xma Ⅰ (100 U mL^{-1} each)). (2) Other four miR-21 analogues with two mutant site in random (Table 1, 1 μM each). Figure 2C shows that the DTB fluorescence intensity changes for the Ago2 and other control proteins which produced fluorescence signals only slightly larger than the background (control column). These results clearly demonstrated that the DTB shows a high selectivity toward Ago2. This high specificity was derived from the cleavage ability of Ago2/miR-21 complex. We next test the selectivity of the miR-21 with other miRNAs. Figure 2D shows the fluorescence changes for the miR-21 and the other four miRNAs treated with Ago2 and DTB. These results clearly demonstrate that the DTB shows a high selectivity toward miR-21. This high specificity with the mismatch discrimination ability was derived from the Ago2 discernment capacity to miR-21, and the recognition ability of loop part of DTB to miRNA.

Measurement of Ago2 in cell lysates. We then challenged our DTB for detecting Ago2 in a complicated sample matrix by spiking different concentration Ago2 into HeLa cell lysates. Box plots in Figure 2E shows the distribution of adding Ago2 in cell lysates with different concentrations (0 nM, 10 nM, 20 nM, 40 nM 60 nM 80 nM and 100 nM). The boxes bound the interquartile range (IQR) by the mean (n=10), and the median and whiskers extend to a maximum of 1.5 × IQR beyond the boxes. The boxes width is scaled to $\sqrt{n}$ (n=10 here). These box plots results showed that the

interference of cell lysates to Ago2 could be overcome by using our DTB. We also determined the endogenous Ago2 concentration by using the fluorescence intensity (284.1) which obtained by measuring cell lysates directly. The endogenous Ago2 concentration determined to be 16.4 nM according to the regression equation of the standard curve in Figure 2B insert. Therefore, DTB exhibits excellent selectivity for Ago2 detection in real samples and has great potential to be applied in clinical tests.

Ago2/miR-21 complex assay by using the DTB in single-cell. Then, we further investigated intracellular Ago2 concentration by using DTB. HeLa cell line was chosen as a model since HeLa cells has a high expression level of Ago2/miR-21 complex.[9] The amount of probe used for Ago2 assay in HeLa cells was first optimized to be 25 μL by flow cytometry (Figure S1). To optimize the suitable imaging time of DTB by investigating different incubation time with HeLa cell. From Figure 3 we can observed that the fluorescence intensity in the cell area increased with the time went by, and the HeLa cell incubated for 4 h reached plateau. So, we use the DTB for the Ago2/miR-21 complex assay in HeLa cells by incubated with 4 h. In addition, to determine whether the fluorescence signals come solely from Ago2, siRNA duplex (Ago2 knockdown siRNA duplex,[9] siRNA1 and siRNA2, Table 1) was introduced to knockdown Ago2 in HeLa cells. In addition, Ago2 inhibits cell proliferation and causes cell to death by decreasing c-Myc expression in cells.[9] So, we verified the Ago2 knockdown reaction by using c-Myc mRNA changes in cells. The fluorescence confocal images and RT-qPCR results shown in Figure S2 indicated that the siRNA duplex induced dramatic decrease of fluorescence intensity through the Ago2

knockdown (Figure S3). These data indicate that intracellular Ago2 activities triggered the fluorescence intensity's generation by acting on the DTB.

Before assay Ago2/miR-21 complex in single cells, the stability of DTB was incubated with DNase I for the cleavage assay in PBS buffer. Compared with the DNA/AgNC fluorescence intensity, the mixture of DTB with DNase (1 U mL^{-1}) showed negligible fluorescence intensity change even after incubation for 6 h (Figure 4), indicating excellent stability and wide intracellular usage.

We next measure the fluorescence intensity in single-cell after incubated with different concentrations (0 nM, 10 nM, 100 nM and 1 μM) DTB for 4 h (Figure 5). the fluorescence intensity gradually increased with the DTB concentration increase. These results demonstrated that our DTB was suitable for imaging Ago2/miR-21 in single-cell.

The feasibility of the DTB for quantification of Ago2 concentration was further verified using other immortalized cells, such as HEK293 (human embryonic kidney cells) and LO2 (human hepatic cells). After incubated with 100 nM DTB for 4 h, the cells were sent for fluorescent confocal imaging detection (Figure S4). We can obtain that the HEK293 cell and LO2 cell all exhibited high fluorescence intensity in the cell areas. The detection results indicated that our DTB was also suitable for imaging Ago2/miR-21 complex in human immortalized cells. Kamiya et al. reported a methodology for the modification of nucleic acids by use of base-surrogates with D-threoninol as the scaffold for the functionalization of siRNAs for the detection of Ago2 concentration in living cells.[11] They employed a function molecule, in which

fluorophore and quencher dyes are dimerized in the stem region for the sensitivity and selectivity assay. However, a relatively long time (24 hours) was utilized for the cell imaging. Compared with this time-consuming strategy, our method has the advantages of "label-free" and less time-needing.

The universality of the DTB. Ribonuclease H (RNase H) plays an importance role in Human immunodeficiency virus type-1 (HIV-1) reverse transcriptase pathway by digesting the RNA strand in RNA/DNA duplex. So, the RNase H concentration in single cells makes it an important factor in anti-HIV drugs research. To demonstrate further the feasibility and universality of the DTB, the biosensor was employed for the further assay RNase H concentration with just a little sequences change at the hairpin part. In addition, Antisense oligonucleotides (ASOs) have been used wildly to knockdown mRNAs by cleaving RNA strand in DNA/RNA heteroduplex. To assay the RNase H concentration by using the DTB, we employed the ASO (the sequences please see Table 1) which have a phosphorothioate backbone with DNA-like bases in the center and modified bases in the wing for the inhibiting pre-Let-7a as a model.[37] As shown in Scheme 2, in the absence of RNase H, the formation of the hairpin structure leads the two PET pairs adjacent to each other, which makes PET on, and no DNA/AgNC fluorescence can be obtained. In the present of RNase H, the hairpin structure can be cleavage by RNase H with the help of ASO. The cleavage reaction also makes the hairpin structure in an open stage, leading the two PET pair spatially separated (PET off). Thus, the DNA/AgNC fluorescence can be observed when excited with the light of 560 nm. Thus, the fluorescence intensity of DNA/AgNC can be used

as a signal transducer for quantitation of RNase H concentration.

We further recorded the fluorescence intensity of the DNA/AgNC when adding different concentration of RNase H (Figure 6A). The fluorescence intensity indicated that as the RNase H concentration increased, the fluorescence emission spectra intensity increased according. Figure 6B shows the relationship of the DNA/Ag NC fluorescence intensity and the concentration of RNase H. The inset part indicated the linearly relationship between the fluorescence intensity (*FL*) and the concentration (C_{RH}) of RNase H over the range from 0 to 100 U mL^{-1} with an equation $FL = 8.53\ C_{RH} + 196.30$ ($R^2 = 0.998$). The limit of detection (LOD) can be calculated as 3.41 U mL^{-1}, which is lower or comparable than previously reports (Table S2). Similarity to the specificity assay in Ago2 assay, DTB was evaluated with the control experiments (argonaute1 (Ago1, 100 nM), argonaute2 (Ago2, 100 nM), argonaute3 (Ago3, 100 nM) and EcoRI (100 U mL^{-1}). Figure 6C shows the fluorescence intensity of DTB by treated with control group proteins and the results demonstrate that the DTB shows a high selectivity toward the RNase H.

The DTB was also employed for the RNase H detection in cell lysis. We employed four human cell lysates (HeLa, A549, PC-3, and MCF-7) and different concentrations of RNase H were added into 10% cell lysis and tested by using our DTB. The fluorescence intensity of cell lysis which treated with different concentration of RNase H were tested by using our DTB. The RNase H concentration were calculated by using the formula in Figure 6B inset. Figure 6D gives the relationship of added RNase H and measured RNase H activities in different cell lysis. By comparing the signal intensities

caused by these samples with the same concdentration, we found that HeLa cell lysis caused the largest fluorescence signal change, which demonstrated that the levels of RNase H in HeLa (about 6.68±0.50 nM) were the highest in these employed cell lines. These results indicate that our DTB hold great promise for RNase H assay in real samples.

CONCLUSION

In conclusion, we have built a DTB for Ago2 and RNase H concentration assay. The DTB have successful been used for Ago2 concentration in single cells. By employed the competition-mediated photo-induced electron transfer (PET) between DNA/AgNCs and G-quadruplex/hemin complexes, the DTB exhibits the advantages of high resistance to degradation, structural stability, and transfection into cells without carriers with a signal-on features. Compared with conventional strategies, our DTB shows some unique features: (1) It is very simple and low cost since the formation DNA-templated silver nanoclusters and the G-quadruplex/hemin complex does not require chemical synthesis. (2) The self-assembly of the DTB formation does not require troublesome makes the process operation is simple. (3) It can be used for multiple protein concentration assay with only small sequences changes in the hairpin part. Therefore, the DTB can be used as a new device for the imaging protein concentration in single cells, and have a potential value for disease diagnosis and treatment, such as cancer and HIV by inhibiting related genes' expression.

ASSOCIATED CONTENT

Supporting Information

The Supporting Information is available free of charge on the ACS Publications website at DOI:

The flow cytometry assay, Ago2 knockdown assay, confocal images of HEK293 and LO2 cells, Table S1and Table S2.

AUTHOR INFORMATION

Corresponding Author

*E-mail: zhangkai@jsinm.org

*E-mail: xieminhao@jsinm.org

Notes

The authors declare no competing financial interest.

ACKNOWLEDGMENTS

This work was supported by the National Natural Science Foundation (21705061), the Jiangsu Provincial Key Medical Discipline (Laboratory) (ZDXKA2016017) and the Innovation Capacity Development Plan of Jiangsu Province (BM2018023).

REFERENCE

(1) Niu, W.; Chen, X.; Tan, W.; Veige, A. S. *Angew. Chem. Int. Ed.* **2016**, *55*, 8889-8893.

(2) Liu, Y.; Zhou, J.; Wang, L.; Hu, X.; Liu, X.; Liu, M.; Cao, Z.; Shangguan, D.; Tan, W. *J. Am. Chem. Soc.* **2016**, *138*, 12368-12374.

(3) Kwok, C. K.; Sahakyan, A. B.; Balasubramanian, S. *Angew. Chem. Int. Ed.* **2016**, *55*, 8958-8961.

(4) Zhang, H.; Ma, Y.; Xie, Y.; An, Y.; Huang, Y.; Zhu, Z.; Yang, C. J. *Sci. Rep.* **2015**, *5*, 10099.

(5) Yuan, Y.; Zhang, C.-J.; Gao, M.; Zhang, R.; Tang, B. Z.; Liu, B. *Angew. Chem. Int. Ed.* **2015**, *54*, 1780-1786.

(6) Yu, T.; Wei, Q. *Nano Research* **2018**, 11, 5439-5473.

(7) Krell, J.; Stebbing, J.; Frampton, A. E.; Carissimi, C.; Harding, V.; De Giorgio, A.; Fulci, V.; Macino, G.; Colombo, T.; Castellano, L. *Lancet* **2015**, *385 Suppl 1*, S15.

(8) Iwasaki, S.; Sasaki, H. M.; Sakaguchi, Y.; Suzuki, T.; Tadakuma, H.; Tomari, Y. *Nature* **2015**, *521*, 533-536.

(9) Zhang, K.; Yang, X.-J.; Zhao, W.; Xu, M.-C.; Xu, J.-J.; Chen, H.-Y. *Chem. Sci.* **2017**, *8*, 4973-4977.

(10) Feng, Q. M.; Zhu, M. J.; Zhang, T. T.; Xu, J. J.; Chen, H. Y. *Analyst* **2016**, *141*, 2474-2480.

(11) Kamiya, Y.; Ito, A.; Ito, H.; Urushihara, M.; Takai, J.; Fujii, T.; Liang, X. G.; Kashida, H.; Asanuma, H. *Chem. Sci.* **2013**, *4*, 4016-4021.

(12) Pecot, C. V.; Calin, G. A.; Coleman, R. L.; Lopez-Berestein, G.; Sood, A. K. *Nat. Rev. Cancer* **2011**, *11*, 59-67.

(13) Felice, K. M.; Salzman, D. W.; Shubert-Coleman, J.; Jensen, K. P.; Furneaux, H. M. *Biochem. J* **2009**, *422*, 329-341.

(14) Chang, C. I.; Yoo, J. W.; Hong, S. W.; Lee, S. E.; Kang, H. S.; Sun, X. G.; Rogoff, H. A.; Ban, C.; Kim, S.; Li, C. J.; Lee, D. K. *Mol. Ther.* **2009**, *17*, 725-732.

(15) Castanotto, D.; Rossi, J. J. *Nature* **2009**, *457*, 426-433.

(16) Carthew, R. W.; Sontheimer, E. J. *Cell* **2009**, *136*, 642-655.

(17) Mi, S.; Cai, T.; Hu, Y.; Chen, Y.; Hodges, E.; Ni, F.; Wu, L.; Li, S.; Zhou, H.; Long, C.; Chen, S.; Hannon, G. J.; Qi, Y. *Cell* **2008**, *133*, 116-127.

(18) Hutvagner, G.; Simard, M. J. *Nat Rev Mol Cell Biol* **2008**, *9*, 22-32.

(19) Frank, F.; Sonenberg, N.; Nagar, B. *Nature* **2010**, *465*, 818-822.

(20) Cifuentes, D.; Xue, H.; Taylor, D. W.; Patnode, H.; Mishima, Y.; Cheloufi, S.; Ma, E.; Mane, S.; Hannon, G. J.; Lawson, N. D.; Wolfe, S. A.; Giraldez, A. J. *Science* **2010**, *328*, 1694-1698.

(21) Zhang, Y.; Shuai, Z.; Zhou, H.; Luo, Z.; Liu, B.; Zhang, Y.; Zhang, L.; Chen, S.; Chao, J.; Weng, L.; Fan, Q.; Fan, C.; Huang, W.; Wang, L. *J. Am. Chem. Soc.* **2018**, *140*, 3988-3993.

(22) Wang, S.; Xia, M.; Liu, J.; Zhang, S.; Zhang, X. *ACS Sensors* **2017**, *2*, 735-739.

(23) Qu, X.; Zhang, H.; Chen, H.; Aldalbahi, A.; Li, L.; Tian, Y.; Weitz, D. A.; Pei, H. *Anal. Chem.* **2017**, *89*, 3468-3473.

(24) Li, N.; Wang, M.; Gao, X.; Yu, Z.; Pan, W.; Wang, H.; Tang, B. *Anal. Chem.* **2017**, *89*, 6670-6677.

(25) He, L.; Lu, D.-Q.; Liang, H.; Xie, S.; Luo, C.; Hu, M.; Xu, L.; Zhang, X.; Tan, W. *ACS Nano* **2017**, *11*, 4060-4066.

(26) Xie, S.; Dong, Y.; Yuan, Y.; Chai, Y.; Yuan, R. *Anal. Chem.* **2016**, *88*, 5218-5224.

(27) Xie, N.; Huang, J.; Yang, X.; Yang, Y.; Quan, K.; Ou, M.; Fang, H.; Wang, K. *ACS Sensors* **2016**, *1*, 1445-1452.

(28) Xia, Z.; Wang, P.; Liu, X.; Liu, T.; Yan, Y.; Yan, J.; Zhong, J.; Sun, G.; He, D. *Biochemistry* **2016**, *55*, 1326-1331.

(29) Song, P.; Li, M.; Shen, J.; Pei, H.; Chao, J.; Su, S.; Aldalbahi, A.; Wang, L.; Shi, J.; Song, S.; Wang, L.; Fan, C.; Zuo, X. *Anal. Chem.* **2016**, *88*, 8043-8049.

(30) Chen, N.; Qin, S.; Yang, X.; Wang, Q.; Huang, J.; Wang, K. *ACS Appl. Mater. Inter.* **2016**, *8*, 26552-26558.

(31) Miao, P.; Wang, B.; Meng, F.; Yin, J.; Tang, Y. *Bioconjugate Chem.* **2015**, *26*, 602-607.

(32) Li, J.; Hong, C.-Y.; Wu, S.-X.; Liang, H.; Wang, L.-P.; Huang, G.; Chen, X.; Yang, H.-H.; Shangguan, D.; Tan, W. *J. Am. Chem. Soc.* **2015**, *137*, 11210-11213.

(33) Li, Z.; Zhao, B.; Wang, D.; Wen, Y.; Liu, G.; Dong, H.; Song, S.; Fan, C. *ACS Appl. Mater. Inter.* **2014**, *6*, 17944-17953.

(34) Abi, A.; Lin, M.; Pei, H.; Fan, C.; Ferapontova, E. E.; Zuo, X. *ACS Appl. Mater. Inter.* **2014**, *6*, 8928-8931.

(35) Wilks, T. R.; Bath, J.; de Vries, J. W.; Raymond, J. E.; Herrmann, A.; Turberfield, A. J.; O'Reilly, R. K. *ACS Nano* **2013**, *7*, 8561-8572.

(36) Zhang, K.; Wang, K.; Zhu, X.; Gao, Y.; Xie, M. *Chem. Commun.* **2014**, *50*, 14221-

14224.

(37) Zhang, L.; Zhu, J.; Guo, S.; Li, T.; Li, J.; Wang, E. *J. Am. Chem. Soc.* **2013**, *135*, 2403-2406.

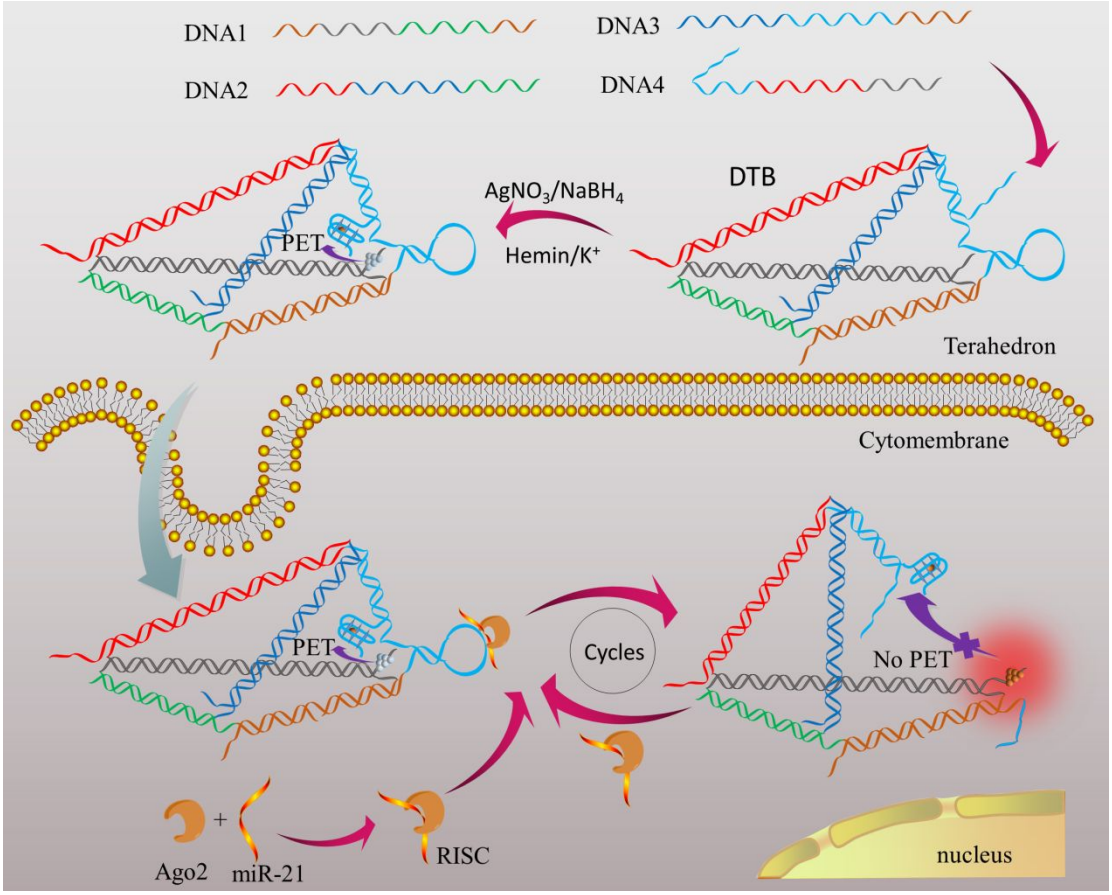

Scheme 1. Schematic diagram showing the procedure of Ago2 assay in single-cell by using the DTB.

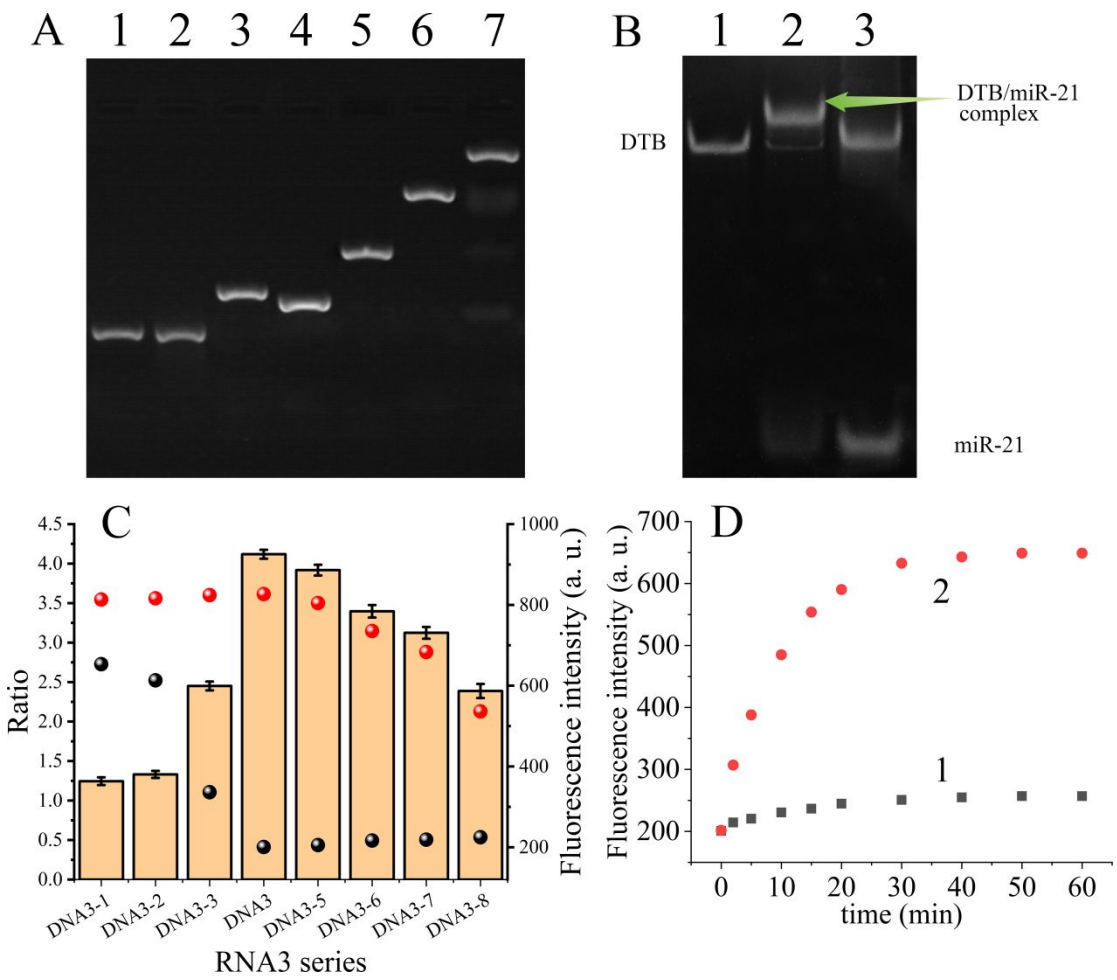

Figure 1. Optimization assay. (A) Nondenaturing polyacrylamide gel electrophoresis (PAGE, 10%) of the products for the preparing of the DTB. Lane (1): DNA1; Lane (2): DNA2; Lane (3): DNA3; Lane (4): DNA4; Lane (5): DNA1 and DNA2; Lane (6): DNA1, DNA2 and DNA3; Lane (7): DNA1, DNA2, DNA3 and DNA4, respectively. (B) Nondenaturing PAGE (10%) assay to verify the Ago2/miR-21 complex cleavage reaction. Lane (1) DTB, (2) DTB/miR-21 complex, (3) DTB/miR-21 treated with 100 nM Ago2. (C) The relationship of the stem part length of the hairpin structure in DNA3 and the ratio of the F_{signal}/F_{blank}. The fluorescence intensity in the absence of Ago2/miR-21 (black points, F_{blank}) and presence of Ago2/miR-21 (red points, F_{signal}) were also list in the figure. (D) Fluorescence intensity *vs*. the time in the presence of 10 nM (1) and 100 nM (2) Ago2.

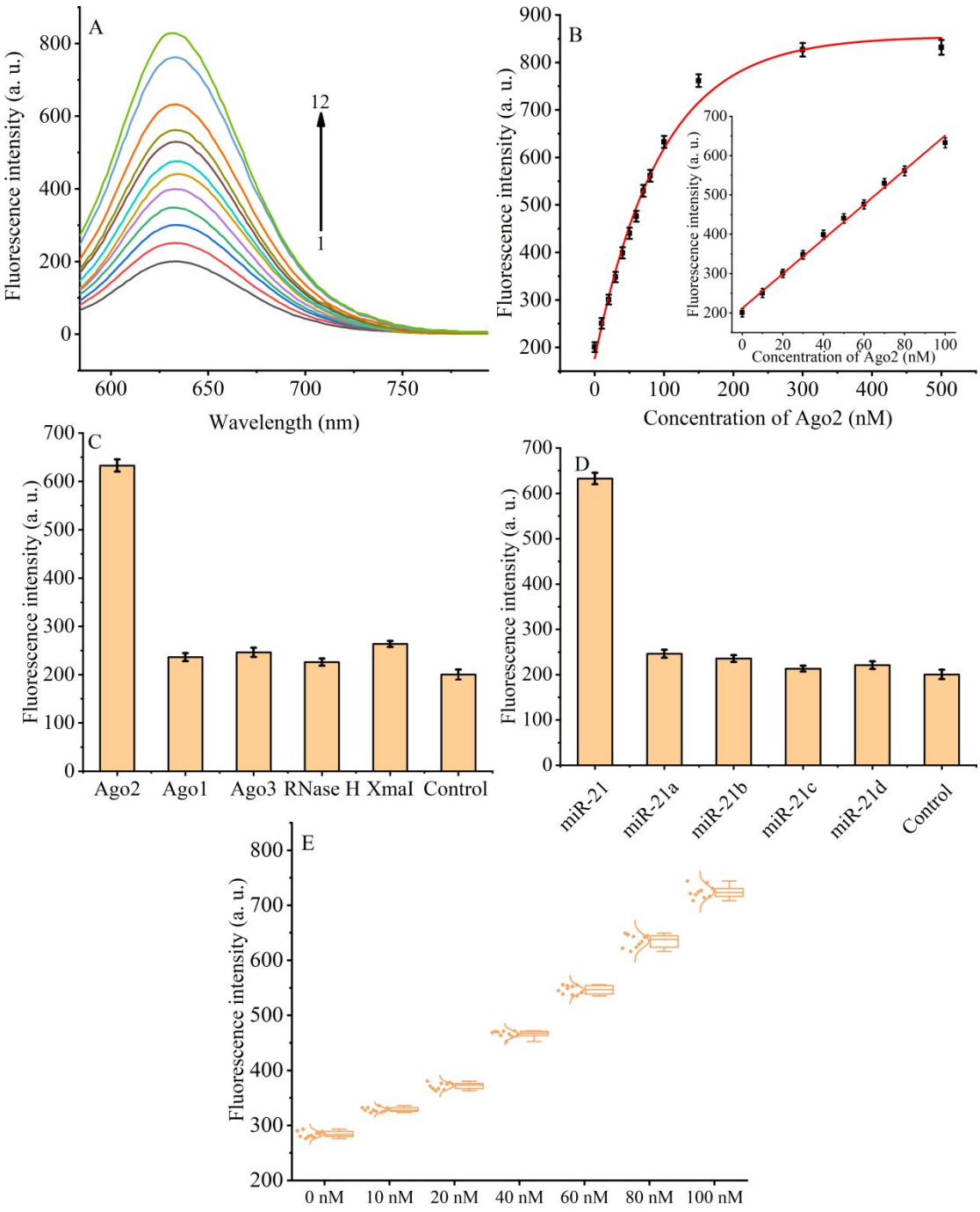

Figure 2. (A) The DNA/AgNC fluorescence spectrum of the DTB by treated with different concentration Ago2 (with 1 μM miR-21): (1) 0 nM, (2) 10 nM, (3) 20 nM, (4) 30 nM, (5) 40 nM, (6) 50 nM, (7) 60 nM, (8) 70 nM, (9) 80 nM, (10)100 nM, (11)150 nM, and (12) 300 nM, respectively. (B) Relationship between the fluorescence intensity at 620 nm and the concentration of Ago2 in buffer. The inset shows the linear relationship over the Ago2 concentration from 0 to 100 nM. All the data in the experiment were obtained from at least three independent experiments

and error bars denote standard deviations (SD). (C) The specificity by using the DTB for the test of Ago2 and other proteins. The concentration of Ago1 and Ago3 are all 100 nM and the RNase H and Xma Ⅰ are all 100 U mL^{-1} (D) The specificity by using the DTB for the test of miR-21 (1 μM) and other miRNAs (1 μM each). (E) Specifically assay by using standard addition method. Box plots of the DTB fluorescence intensity measured by adding different concentration Ago2 (0 nM, 10 nM, 20 nM, 40 nM 60 nM 80 nM and 100 nM) to cell lysis.

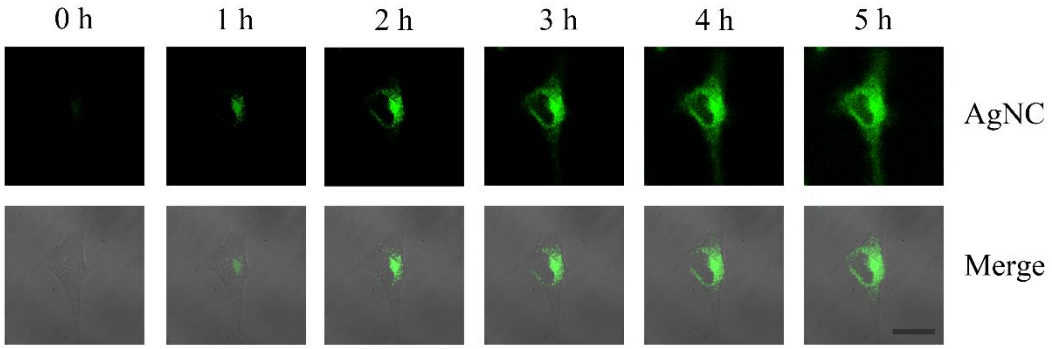

Figure 3. Time course of confocal images of HeLa cells incubated with 25 μL of DTB (scale bar 25 μm).

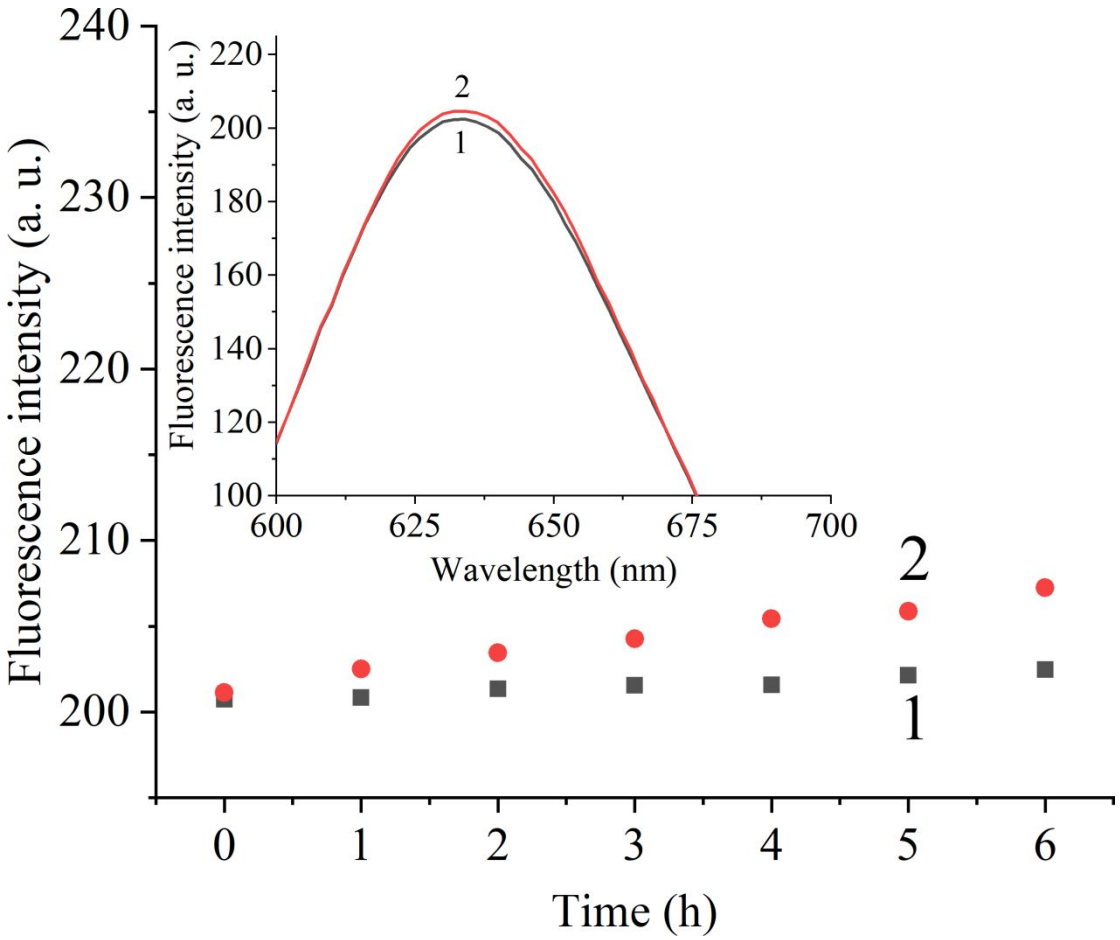

Figure 4. Plots of DNA/AgNC fluorescence intensity at 620 nM of the DTB in absence (1) and presence (2) of 1 U mL^{-1} DNase I vs. incubation time. Inset: fluorescence spectra corresponding to plots 1 and plots 2 at 6 h.

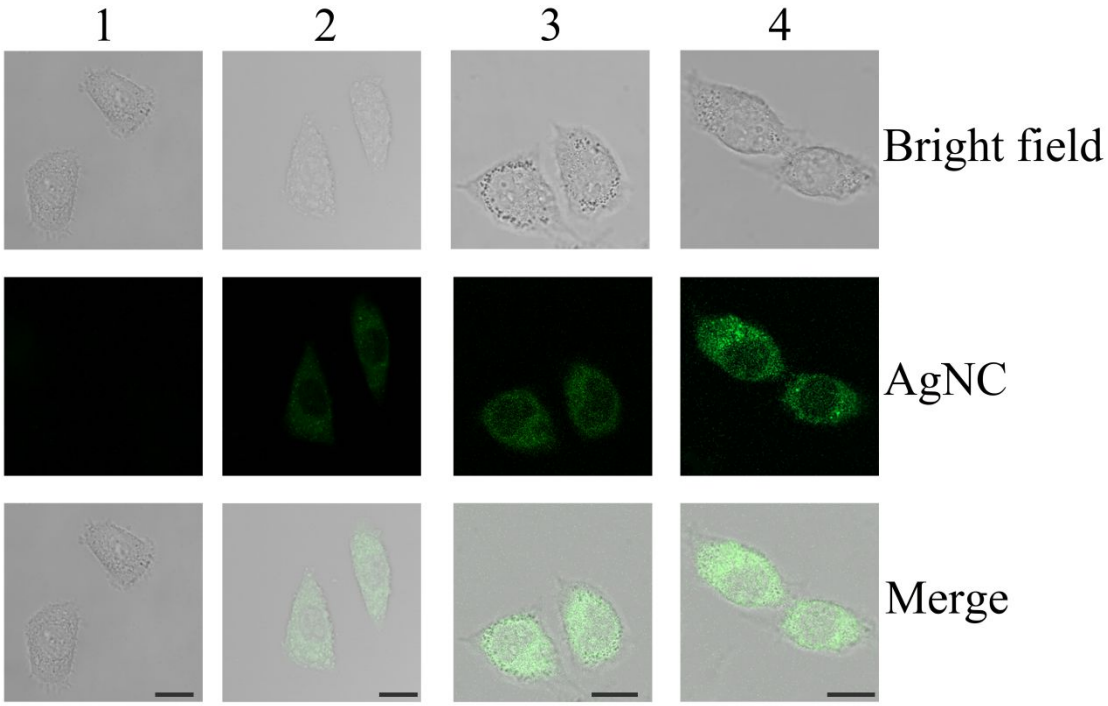

Figure 5. Confocal images of HeLa cells after incubation with 25 μL of DTB for 4 h with different concentrations: (1) 0 nM, (2) 10 nM, (3) 100 nM, and (4) 1 μM, respectively. (Scale bar 25 μm).

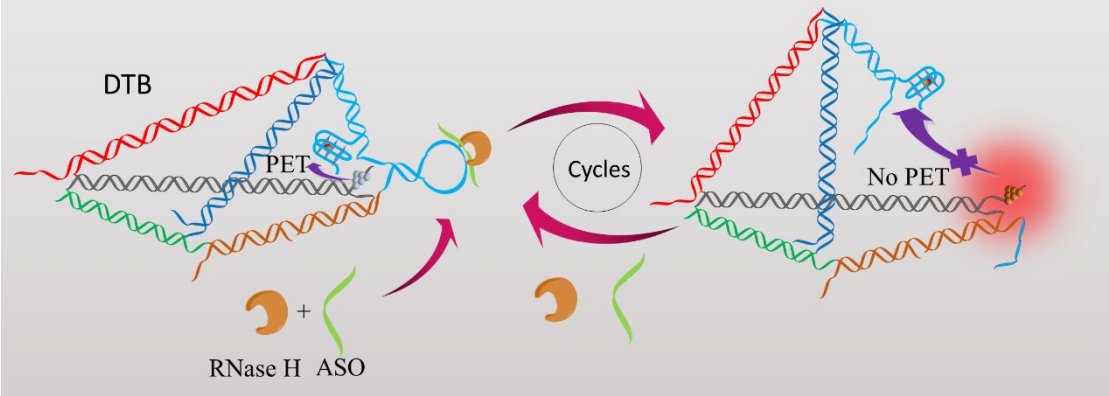

Scheme 2. Schematic diagram showing the procedure of RNase H assay *in situ* by using the DTB.

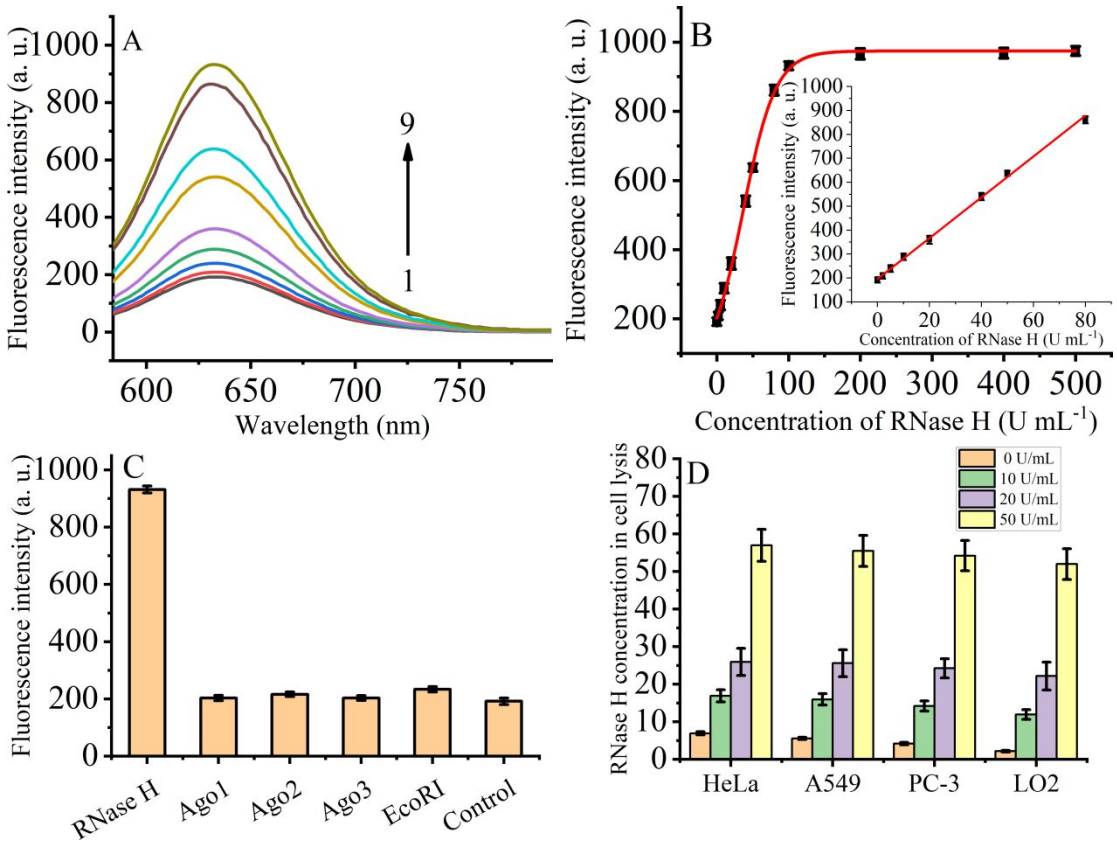

Figure 6. (A) The DNA/AgNC fluorescence spectrum of the DTB by treated with different concentration RNase (with 1 μM Let-7a): 0, 2, 5, 10, 20, 40, 50, 80, and 100 U mL^{-1} from curve 1 to 9, respectively. (B) Relationship between the fluorescence intensity at 620 nM and the concentration of RNase H. The inset shows the linear relationship over the RNase H concentration from 0 to 80 U mL^{-1}. (C) The specificity by using the DTB for the test of RNase H and other proteins. (D) Measured RNase H activities in cell lysis after added different concentration RNase H (0, 10, 20, and 50 U mL^{-1}). All the data in the experiment were obtained from at least three independent experiments and error bars denote standard deviations (SD).

Table 1. Sequence information for the sequences used in this study. The underlined sequence in DNA3, DNA3' and DNA3-1 to DNA3-8 is the hairpin structure. The italic is the stem part. The sequence shown in bold in DNA4 is used to form the AgNC and the double-underlined sequence is used for G-quadruplex/hemin complex formation. The italic letter in miR-21a, miR-21b, miR-21c and miR-21d indicate the mutation base. The * labelled sequence is the ASO.

note	sequence (5' to 3')
DNA1	CTTGCTACACGATTCAGACTTAGGAATGTTCGACATGCGAGGGTCCAA TACCGACGATTACAG
DNA2	ACGAACATTCCTAAGTCTGAAATTTATCACCCGCCATAGTAGACGTAT CACCAGGCAGTTGAG
DNA3	ACGTGTAGCAAGCTGTAATCGACT*GCGG*TTTTTGUAGCUUAUCAGACU GAUGUUGTTTTT*CCGC*TCGGCTCACTACTATGGCGGGTGATAAA
DNA3-1	CGTGTAGCAAGCTGTAATCGACT*G*TTTTTGUAGCUUAUCAGACUGAUG UUGTTTTT*C*TCGGCTCACTACTATGGCGGGTGATAAA
DNA3-2	CGTGTAGCAAGCTGTAATCGACT*GC*TTTTTGUAGCUUAUCAGACUGAU GUUGTTTTT*GC*TCGGCTCACTACTATGGCGGGTGATAAA
DNA3-3	CGTGTAGCAAGCTGTAATCGACT*GCG*TTTTTGUAGCUUAUCAGACUGA UGUUGTTTTT*CGC*TCGGCTCACTACTATGGCGGGTGATAAA
DNA3-5	CGTGTAGCAAGCTGTAATCGACT*GCGCG*TTTTTGUAGCUUAUCAGACU

	GAUGUUGTTTTT*CGCGC*TCGGCTCACTACTATGGCGGGTGATAAA
DNA3-6	CGTGTAGCAAGCTGTAATCGACT*GCGGCG*TTTTTGUAGCUUAUCAGAC UGAUGUUGTTTTT*CGCCGC*TCGGCTCACTACTATGGCGGGTGATAAA
DNA3-7	CGTGTAGCAAGCTGTAATCGACT*GCCGGCG*TTTTTGUAGCUUAUCAGA CUGAUGUUGTTTTT*CGCCGGC*TCGGCTCACTACTATGGCGGGTGATAA A
DNA3-8	CGTGTAGCAAGCTGTAATCGACT*GCCGGGCG*TTTTTGUAGCUUAUCAG ACUGAUGUUGTTTTT*CGCCCGGC*TCGGCTCACTACTATGGCGGGTGAT AAA
DNA4	**CCTCCTTCCTCCT**ACGGTATTGGACCCTCGCATGACTCAACTGCCTGG TGATACGAGAGCCGAATTGGGTAGGGCGGGTTGGG
DNA3’	ACGTGTAGCAAGCTGTAATCGACT*GCGG*TTTTTAACUAUACAACCUAC UACCUCATTTTTT*CCGC*TCGGCTCACTACTATGGCGGGTGATAAA
miR-21	CAACAUCAGUCUGAUAAGCUAC
miR-21a	CAACAUCAG*C*CU*A*AUAAGCUAC
miR-21b	CAACAUCAGUCUGAUAA*U*CU*C*C
miR-21c	CA*G*CAU*A*AGUCUGAUAAGCUAC
miR-21d	CAACAUCAGUCUG*G*UAA*U*CUAC
ASO	*T*G*A*G*G*T*T*A*G*T*A*G*G*T*T*T*G*T*A*T*A*G*T*T
siRNA1	CGAUCGGCAAGAAGAGAUUAG
siRNA2	AAUCUCUUCUUGCCGAUCGGG

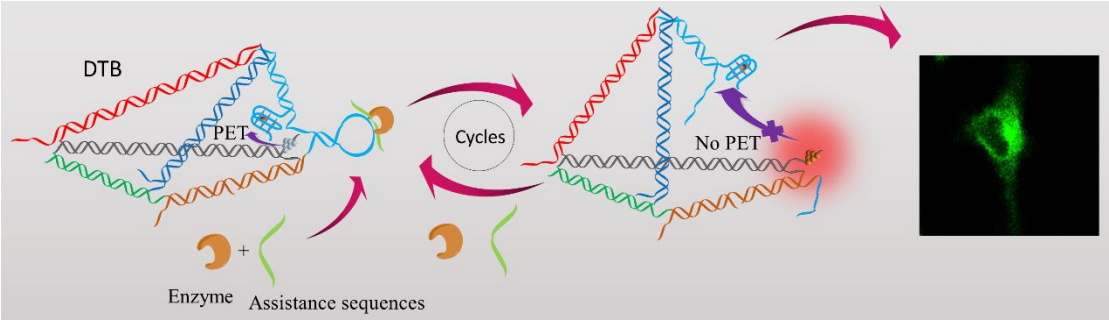

For TOC only.

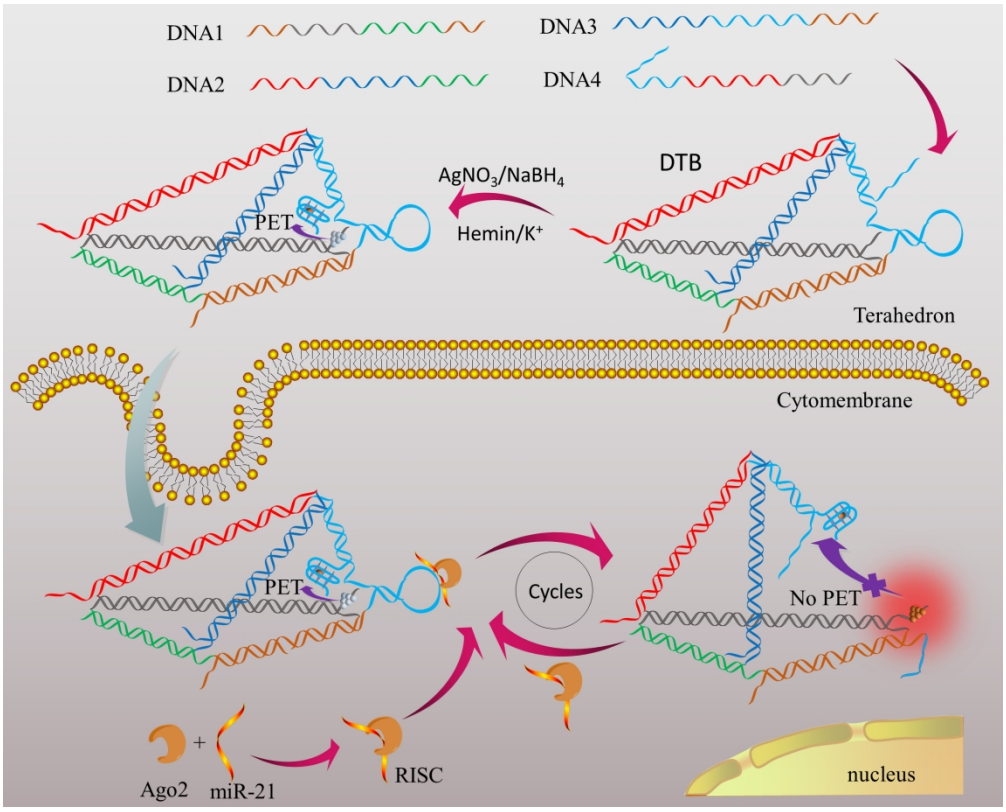

Scheme 1. Schematic diagram showing the procedure of Ago2 assay in single-cell by using the DTB.

633x508mm (96 x 96 DPI)

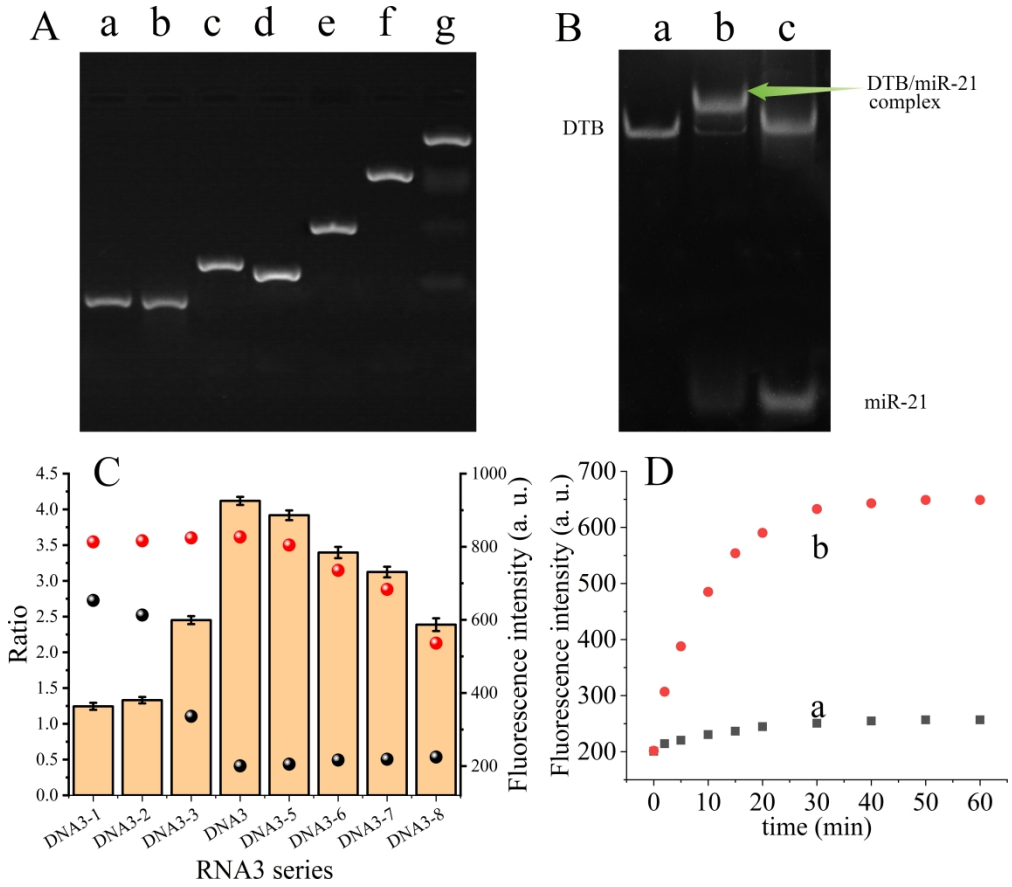

Figure 1. Optimization assay. (A) Nondenaturing polyacrylamide gel electrophoresis (PAGE, 10%) of the products for the preparing of the DTB. Lane (a): DNA1; Lane (b): DNA2; Lane (c): DNA3; Lane (d): DNA4; Lane (e): DNA1 and DNA2; Lane (f): DNA1, DNA2 and DNA3; Lane (g): DNA1, DNA2, DNA3 and DNA4, respectively. (B) Nondenaturing PAGE (10%) assay to verify the Ago2/miR-21 complex cleavage reaction. Lane (a) DTB, (b) DTB/miR-21 complex, (C) DTB/miR-21 treated with 100 nM Ago2. (C) The relationship of the stem part length of the hairpin structure in DNA3 and the ratio of the Fsignal/Fblank. The fluorescence intensity in the absence of Ago2/miR-21 (black points, Fblank) and presence of Ago2/miR-21 (red points, Fsignal) were also list in the figure. (D) Fluorescence intensity vs. the time in the presence of 10 nM (a) and 100 nM (b) Ago2.

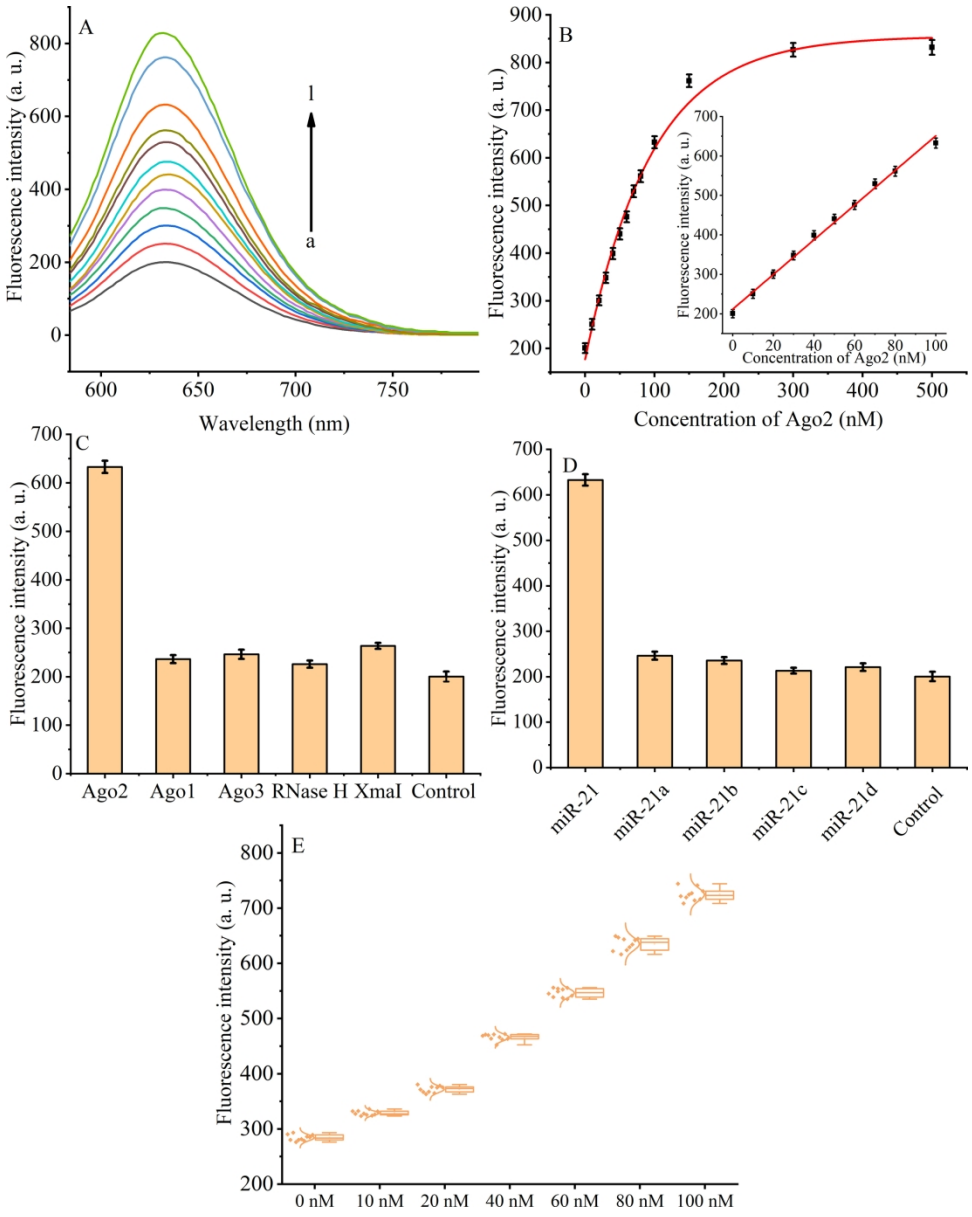

Figure 2. (A) The DNA/AgNC fluorescence spectrum of the DTB by treated with different concentration Ago2 (with 1 μM miR-21): (a) 0 nM, (b) 10 nM, (c) 20 nM, (d) 30 nM, (e) 40 nM, (f) 50 nM, (g) 60 nM, (h) 70 nM, (i) 80 nM, (j)100 nM, (k)150 nM, and (l) 300 nM, respectively. (B) Relationship between the fluorescence intensity at 620 nm and the concentration of Ago2 in buffer. The inset shows the linear relationship over the Ago2 concentration from 0 to 100 nM. All the data in the experiment were obtained from at least three independent experiments and error bars denote standard deviations (SD). (C) The specificity by using the DTB for the test of Ago2 and other proteins. The concentration of Ago1 and Ago3 are all 100 nM and the RNase H and Xma I are all 100 U mL-1 (D) The specificity by using the DTB for the test of miR-21 (1 μM) and other miRNAs (1 μM each). (E) Specifically assay by using standard addition method. Box plots of the DTB fluorescence intensity measured by adding different concentration Ago2 (0 nM, 10 nM, 20 nM, 40 nM 60 nM 80 nM and 100 nM) to cell lysis.

203x253mm (300 x 300 DPI)

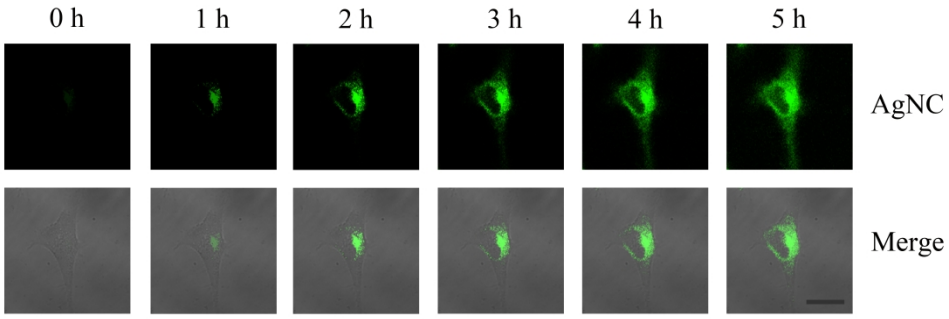

Figure 3. Time course of confocal images of HeLa cells incubated with 25 μL of DTB (scale bar 25 μm).

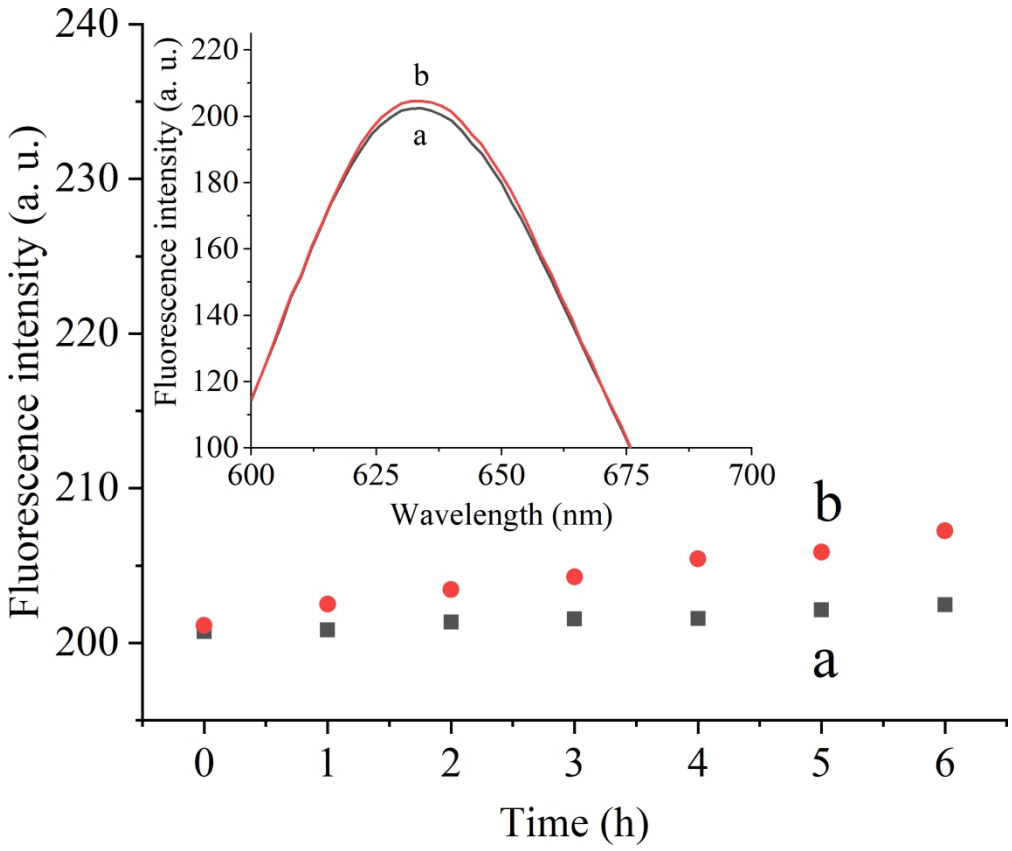

Figure 4. Plots of DNA/AgNC fluorescence intensity at 620 nM of the DTB in absence (a) and presence (b) of 1 U mL-1 DNase I vs. incubation time. Inset: fluorescence spectra corresponding to a and b at 6 h.

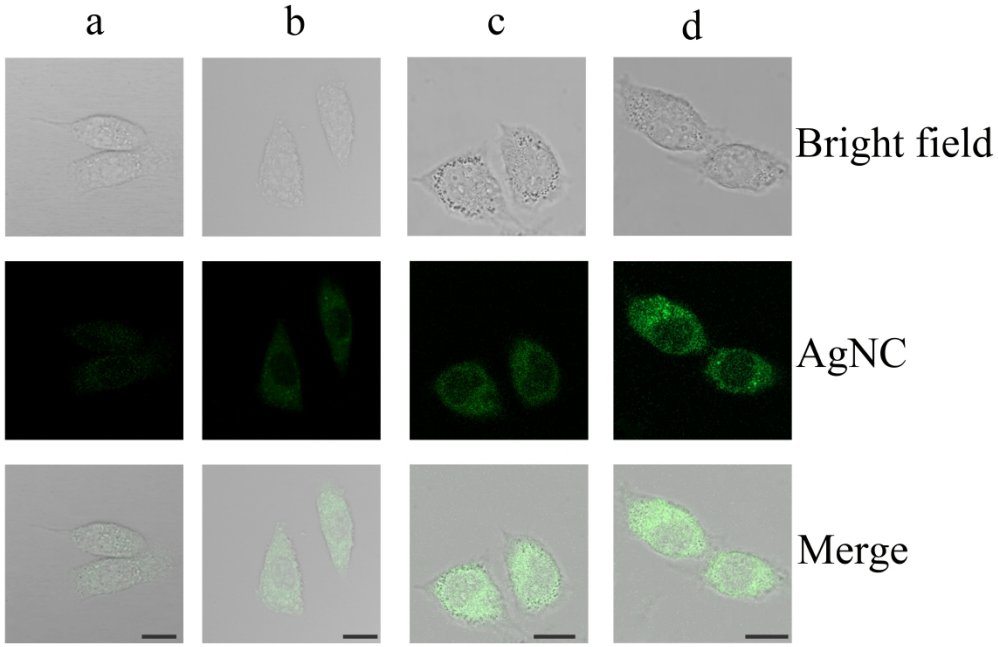

Figure 5. Confocal images of HeLa cells after incubation with 25 μL of DTB for 4 h with different concentrations: (a) 0 nM, (b) 10 nM, (c) 100 nM, and (d) 1 μM, respectively. (Scale bar 25 μm).

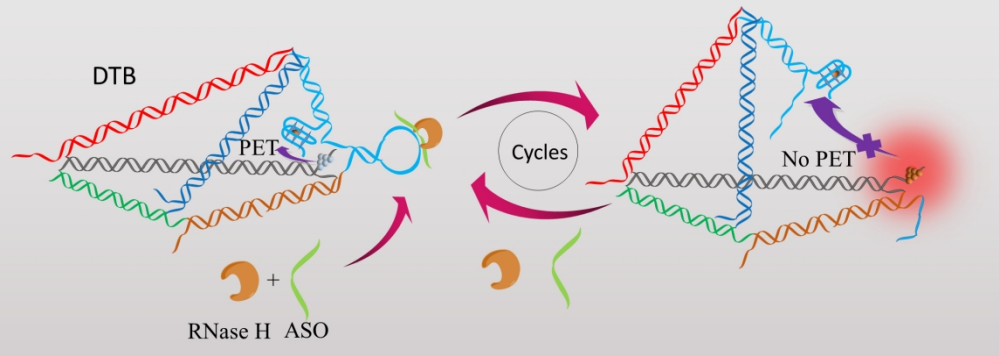

Scheme 2. Schematic diagram showing the procedure of RNase H assay in situ by using the DTB.

612x219mm (96 x 96 DPI)

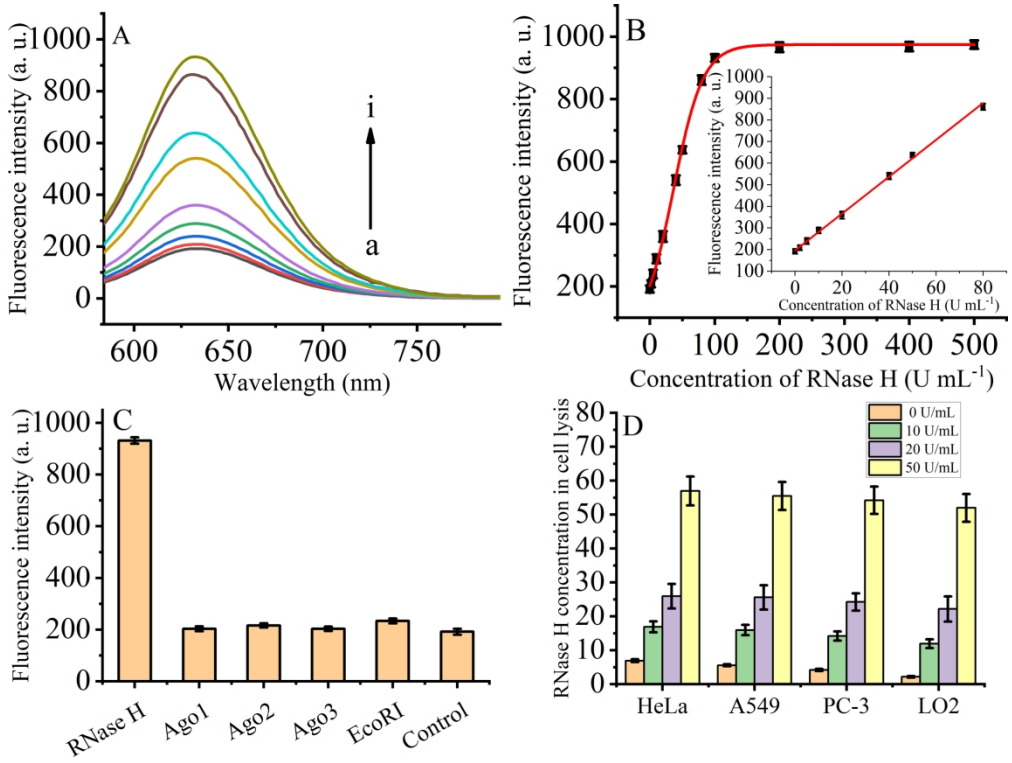

Figure 6. (A) The DNA/AgNC fluorescence spectrum of the DTB by treated with different concentration RNase (with 1 μM Let-7a): 0, 2, 5, 10, 20, 40, 50, 80, and 100 U mL-1 from a to i, respectively. (B) Relationship between the fluorescence intensity at 620 nM and the concentration of RNase H. The inset shows the linear relationship over the RNase H concentration from 0 to 80 U mL-1. (C) The specificity by using the DTB for the test of RNase H and other enzymes. (D) Measured RNase H activities in cell lysis after added different concentration RNase H (0, 10, 20, and 50 U mL-1). All the data in the experiment were obtained from at least three independent experiments and error bars denote standard deviations (SD).

193x145mm (300 x 300 DPI)